Article

Not peer-reviewed version

Sensitivity of Optical Satellites to Estimate Windthrow Tree-Mortality in a Central Amazon Forest

Luciano Emmert *, Robinson Isaac Negrón-Juárez, Jeffrey Quintin Chambers, Joaquim dos Santos, Adriano José Nogueira Lima, Susan Trumbore, Daniel Magnabosco Marra *

Posted Date: 23 May 2023

doi: 10.20944/preprints202305.1631.v1

Keywords: blowdowns; crown damage; forest inventory; extreme wind gusts; natural disturbances; spatial resolution; Spectral Mixture Analysis

Article

Sensitivity of Optical Satellites to Estimate Windthrow Tree-Mortality in a Central Amazon Forest

Luciano Emmert [1,*], Robinson Isaac Negrón-Juárez [2], Jeffrey Quintin Chambers [3], Joaquim dos Santos [4], Adriano José Nogueira Lima [5], Susan Trumbore [6] and Daniel Magnabosco Marra [7,*]

[1] Forest Management Laboratory, National Institute of Amazon Research, Manaus, Amazonas, Brazil; lucianoemmert@yahoo.com.br
[2] Climate Sciences Department, Lawrence Berkeley National Laboratory, Berkeley, California, United States of America; robinson.inj@lbl.gov
[3] Climate Sciences Department, Lawrence Berkeley National Laboratory, Berkeley, California, United States of America; jchambers@lbl.gov
[4] Forest Management Laboratory, National Institute of Amazon Research, Manaus, Amazonas, Brazil; joca@inpa.gov.br
[5] Forest Management Laboratory, National Institute of Amazon Research, Manaus, Amazonas, Brazil; adrianolmf@gmail.com
[6] Biogeochemical Processes Department, Max Planck Institute for Biochemistry, Jena, Germany; trumbore@bgc-jena.mpg.de
[7] Biogeochemical Processes Department, Max Planck Institute for Biochemistry, Jena, Germany; dmarra@bgc-jena.mpg.de
* Correspondence: lucianoemmert@yahoo.com.br (LE) and dmarra@bgc-jena.mpg.de (DMM);

Abstract: Windthrow (i.e., trees broken and uprooted by wind) is a major natural disturbance in the Amazon. Images from medium-resolution optical satellites (mostly Landsat) combined with extensive field data have allowed researchers to assess patterns of tree mortality and monitor forest recovery over decades of subsequent succession in different regions. Although satellites with high spatial-resolution have become available for the Amazon in the last decade, they have not yet been employed for the mapping and quantification of windthrow tree-mortality. Here, we address how increasing the spatial resolution of satellites affects plot-to-landscape estimates of windthrow tree-mortality. We combined forest inventory data with Landsat 8 (30 m pixel), Sentinel 2 (10 m), and WorldView 2 (2 m) imagery over an old-growth forest in the Central Amazon that was disturbed by a single windthrow event in November/2015. Remote sensing estimates of tree mortality were produced with Spectral Mixture Analysis and analyzed together with forest inventory data using Generalized Linear Models. Windthrow tree-mortality measured in 3 transects (30 subplots) crossing the entire disturbance gradient was 26.9 ± 11.1% (mean ± 95% CI). Based on this ground truth, the three satellites produced reliable and statistically similar estimates (from 26.5% to 30.3% windthrow tree-mortality, $p<0.001$). The mean-associated uncertainties decreased systematically with increasing spatial resolution (i.e., from Landsat 8 to Sentinel 2 and WorldView 2). However, the overall quality of fit of models showed the opposite pattern, which may reflect the influence of crown damage not accounted for in our field study, and fast-growing regeneration of leaf area. Among the satellites studied, Landsat 8 most accurately captured field observations of variations in tree mortality across the disturbance gradient (i.e., lower under- and/or overestimation from undisturbed to extremely damaged forest). Although satellites with high spatial-resolution can refine estimates of windthrow severity by allowing the quantification of individual tree damage and mortality, our results validate the reliability of Landsat imagery for assessing patterns of windthrow tree-mortality in dense and heterogeneous tropical forests. Although high-resolution imagery may improve estimates of tree damage and mortality, these should be validated using field data at compatible scales.

Keywords: blowdowns; crown damage; forest inventory; extreme wind gusts; natural disturbances; spatial resolution; spectral mixture analysis

 doi:10.20944/preprints202305.1631.v1

1. Introduction

Windthrows (i.e., trees snapped and uprooted by wind) are the major mechanism of tree-mortality in the Amazon and can influence forest structure, species composition, and carbon balance [1–4]. Optical satellite imagery with medium spatial-resolution (10 m – 39.9 m pixel size) [5] such as Landsat combined with field data has allowed researchers to assess patterns of tree damage and mortality, and monitor forest recovery over decades of subsequent succession in different regions [6–8]. These studies demonstrated that windthrows affect a large portion of the Amazon and occur with a range of intensities and sizes. The Central and Northwestern regions of Amazon Basin concentrate the highest incidence of large-scale (>30 ha) events [6,9,10].

Landsat offers broad coverage of the Earth's surface and long-term imagery data [11–13], allowing reliable estimates of windthrow tree-mortality at the stand, landscape and regional scales [6,7,10]. However, robust estimates of tree-mortality depend on the compatibility between the spatial resolution of optical sensors and the grain size of targets [14,15]. For this reason, identifying windthrows formed by clusters less than ~ 6-8 dead trees is hard with Landsat [16]. Even for larger windthrows (>5 ha), Landsat assessments may underestimate tree-mortality by not accurately capturing relatively lower levels of disturbance on the periphery of highly impacted patches or due to survivoring trees and the relative fast regrowth of the natural regeneration [6,17].

Providing reliable estimates of tree-mortality using remote sensing approaches is not a trivial task. The quality of such estimates is highly dependent on the target of interest (e.g., single tree or clustered trees, [18,19]), the methods used to capture the disturbance information [20] and the sensor characteristics, such as spatial, temporal and spectral resolutions [14,21,22]. The spatial resolution of satellites has been treated as an important variable in this process as it can improve the capability to detect small vegetation damage and minimize the impact of spectral mixing [23]. The spectral mixing tends to dilute the spectral signature of damage/tree mortality with other elements within the pixel, such as shadow, exposed soil or live trees [20,24]. High spatial-resolution satellite data, such as QuickBird, IKONOS, GeoEye, and WorldView, are suitable for detecting small canopy gaps in tropical forests [25–29] and have been shown to be efficient even for detecting individual mortality events in the Amazon [18,19,27,30,31].

Previous studies have related windthrow tree mortality recorded by forest inventories to spectral information extracted from Spectral Mixture Analysis (SMA, [20]) of Landsat images over a wide disturbance gradient [6,7,9]. These studies show a consistent correlation between field and remote sensing data. Although optical satellites with high spatial-resolution (pixel size ≤ 10 m) have become available for the Amazon in the last decade, they have not yet been applied for mapping and estimating windthrow tree-mortality. Therefore, how windthrow tree-mortality estimates obtained with high-resolution satellites will be related to ground truth (i.e., precision and accuracy) in dense tropical forests remains unexplored.

Windthrows are associated with extreme rainfall events produced by mesoscale convective systems [32]. Under climate change, the intensity and frequency of convective storms is predicted to increase [33,34]. Thus, accurately quantifying the occurrence of windthrows and associated tree damage and mortality can contribute to understanding the ecosystem effects of this major disturbance, and to predict how Amazon forests will respond to altered disturbance regimes [35–38].

Here, we combine optical remote sensing with forest inventory data across a disturbance gradient created by a single windthrow event from 2015 to investigate how spatial resolution affects the accuracy and precision of tree-mortality estimates in Central Amazon. Our study provides a framework for future research aiming to access the severity of natural disturbances through reliable estimates of tree-mortality. We addressed the following questions: (i) How does spatial resolution affect estimates of windthrow tree-mortality? (ii) Which sensor (i.e., Landsat 8, Sentinel 2, and WorldView 2) produces the most reliable estimates of tree-mortality across an extent gradient of windthrow severities?

2. Materials and Methods

 doi:10.20944/preprints202305.1631.v1

2.1. Study Area and Sampling Design

The research was conducted in an old-growth forest in Central Amazon, located near the city of Manaus, Brazil (2°53'41"S, 60°16'26"W). This forest was impacted by a convective storm occurred in November 2015, which propagated destructive wind gusts and caused widespread tree-mortality across an area of ~70 hectares (Figure 1a, b, and c).

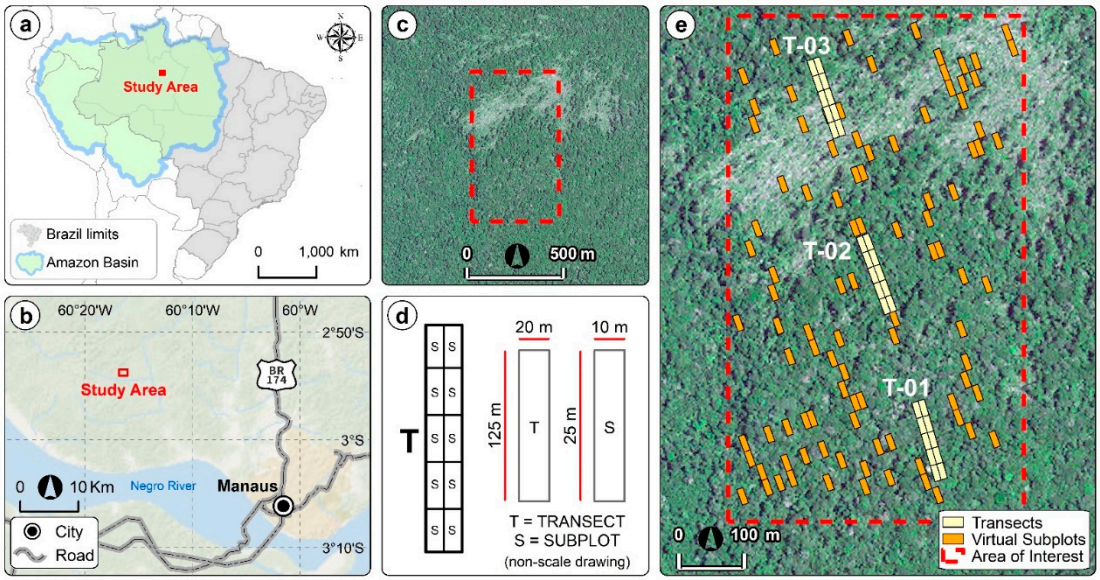

Figure 1. Windthrown forest located in Central Amazon and inventory plots used to quantify tree mortality. (a, b, and c) Location of study area in the Central Amazon, near Manaus, Brazil. (c) Areas of old-growth forest impacted by the 2015 windthrow inside the study area (red dotted polygon). (d and e) Field and virtual subplots for which windthrow tree-mortality was estimated. In (c) and (e) we used a WorldView 2 RGB-composition.

The local relief in our study region is undulating, including plateaus, slopes and small valleys associated with perennial drainages [39,40]. The windthrown area is covered by a forest transitioning from *terra-firme* dominating plateaus to *campinarana* on the slopes and valley bottoms, such as described in adjacent areas [41–44]. In this type of forest, a high diversity of tree species can be found, for instance, from 63 to 137 species in a single hectare [41]. The average annual temperature and annual precipitation in the region of Manaus (40 km from our study site) is 26.9 ± 0.17º C e 2.231 ± 118 mm (mean ± 95% confidence interval for period of 1970-2016, [2]). This region has an evident dry season from July to September, with monthly precipitation less than 100 mm [6,9]. Soils on the plateaus have generally high clay content transitioning to sandy soils in the lower portions that are seasonally flooded [40,45]. In general, the soils have low fertility, low pH, high aluminum concentration and low organic carbon content [39].

To quantify windthrow tree-mortality in the field we carried out a detailed forest inventory following a protocol built up from previous studies [1,2,6,7,16]. The forest inventory was completed in two campaigns, conducted in December 2016 (~ one year after the windthrow) and April 2017 (~ one and a half years after the windthrow). We established three 20 m x 125 m transects, subdivided into 10 subplots of 10 m x 25 m (250 m²) each (total of 30 subplots, referred here as *field subplots*).

Our transects crossed the entire disturbance gradient, ranging from areas with little or no disturbance (i.e., unimpacted old-growth forest) to severely impacted forest with few or no survivor trees. In the field subplots, we recorded, identified and measured the diameter at breast height (DBH) all living trees with DBH ≥10 cm. Due to logistics and safety of our field crew, and for reducing random errors due to possible missing trees hidden by the large amount of coarse wood debris typical of windthrows (Figures S1 to S4) [1,7], we did not count dead trees in severely impacted areas. Instead, we estimated the number of dead trees by subtracting the number of remaining living trees recorded in each subplot from the mean tree density of living trees in old-growth forests in our study

 doi:10.20944/preprints202305.1631.v1

region (i.e., ~ 600 trees.ha^{-1}, or 15 trees in 250 m^2, Table S1, [41–43,46–48]). The subplots with more than 15 recorded living-trees were considered as undisturbed (i.e., no associated windthrow tree-mortality).

2.2. Spectral Mixture Analysis and Remote Sensing Estimates of Windthrow Tree-Mortality

We used Landsat 8, Sentinel 2 satellite imagery acquired before and after the studied windthrow event. For the WorldView 2 satellite, we used only data acquired after the event. Landsat 8 and Sentinel 2 were downloaded from the *Google Earth Engine* platform (https://earthengine.google.com/) [49]. WorldView 2 was purchased from Digital Globe. We selected images with the minimum percent cloud-cover, the closest pass dates to each other and the greatest proximity between the acquisition date and the occurrence of the studied windthrow (Table S2).

We used Spectral Mixture Analysis (SMA) [50,51] to quantify the fractions of endmembers [20] following the routine of previous studies [6,7,9,16,36]. We used the endmembers *photosynthetic vegetation* (GV), *non-photosynthetic vegetation* (NPV), and *shade* (SHD) [20]. The endmembers contain specific spectral signatures of multiple elements that make up the forest surface, and can be used to compute fraction-images on different targets of interest [52,53].

We used an analytical routine on the ENVI 5.3 software to extract the endmembers within each image in a standardized way [20,54–56]. We corrected the scales of Top of the Atmosphere (TOA) reflectance at the pixel level to allow a direct comparison between satellites. Sentinel 2 images are delivered in TOA values divided by 10^{-4}. Worldview 2 requires a band-by-band radiometric correction factor [57] to bring pixel values to the same range as Landsat 8 and Sentinel 2.

As the evaluated satellites have different number of bands and respective spectral ranges, we used the bands common to all of them to obtain the spectral signatures of the endmembers. For Landsat 8 and Sentinel 2 we use the blue, green, red, NIR and SWIR bands. For Worldview 2, due to the smaller spectral range, we use the blue, green, red, red edge and NIR bands. The selected bands are sensitive to the physical, chemical and anatomical characteristics of the leaves and trunks, maximizing the distinction between GV and NPV [50,52,53].

We used a spectral toolkit ([58], Figure S8) to select the purest pixels in all images (e.g. areas where all trees were downed versus unaffected old growth forest canopy) to acquire the most accurate/representative endmembers of interest [20]. Finally, we conducted a SMA to compute the GV, NPV and SHD fraction-images [51] covering our study area.

Windthrows have a specific spectral signature for the NPV fraction, which is originated from the deposition of large amounts of leaves, branches and trunks on the forest floor [59]. To ensure that the GV fraction represented forest patches not affected by the studied windthrow, we selected endmembers within the adjacent old growth forest. The SHD endmember was selected from rivers in the vicinity of the impacted area. To generate final images, the NPV fractions were normalized without SHD as:

$$NPV_{norm} = \frac{NPV}{(GV + NPV)} \quad (1)$$

where NPV_{norm} is the normalized values of the endmembers ranging from 0 to 1 [20]. The best fraction images were selected according to [60], but also based on field observations and the spatial distribution of NPV_{norm} values with respect to windthrow patches visible in a RGB composition. We checked the histograms of the NPV_{norm} fraction-images and we selected images that had more than 98% of the pixels with values between 0 and 1 [61]. We also used the residual error (RMS) from the SMA as a selection criterium (i.e., the lower the better) (Figure 2).

 doi:10.20944/preprints202305.1631.v1

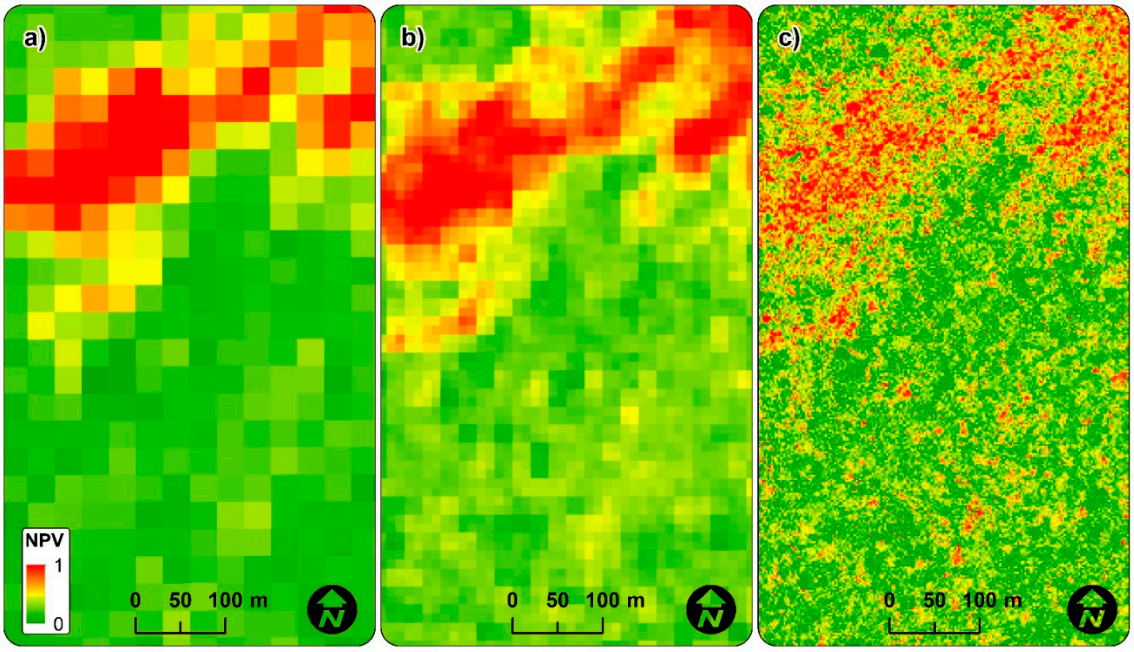

Figure 2. Selected NPV-fraction images from Spectral Mixture Analysis for (a) Landsat 8, (b) Sentinel 2, and WorldView 2.

The differences between the NPV_{norm} before (i.e., old-growth) and after disturbance (ΔNPV) provide a quantitative measure of tree-mortality due the windthrow [36,62]. The larger the ΔNPV values, the greater is the windthrow tree-mortality [7,16,36]. To assess whether the NPV signal was influenced by previous disturbances such as selective logging [61] and human-caused deforestation [63,64], for Landsat 8 and Sentinel 2 we calculated the ΔNPV fraction using a pair of images acquired before and after the studied windthrow date (Table S6). This approach was not used for WorldView 2 as we did not have access to an image before the windthrow. Since NPV_{norm} and ΔNPV for Landsat 8 and Sentinel 2 showed similar amplitude and range of values (Figure S5, Figure S6, Figure S7, Table S4, Table S5, Table S6), and a stable agreement, subsequent analysis with the three sensors were conducted based on the NPV_{norm}.

We calculate a NPV_{norm} value to each field subplot (Table S3). For this, we converted NPV_{norm} fraction images in raster format to NPV_{norm} polygons in shapefile format using QGIS [65]. After that, we overlayed the subplot shapefile with the NPV_{norm} polygons for isolating all segments inside respective subplots. Thus, for each field subplot we obtained one or more segments of NPV_{norm}. We calculated the area of each NPV_{norm} polygon to obtain a weighted NPV value for each subplot [1,2,4] as:

$$NPV = \frac{NPV_{norm} * A}{250} \quad (2)$$

where NPV is the weighted value within each subplot, NPV_{norm} is the normalized value of each pixel and A is the area of each pixel (m^2) that is fully or partially included in the respective subplot; 250 is equivalent to the area (m^2) of each subplot.

Apart from the 30 field subplots, we estimated windthrow tree-mortality remotely for 100 virtual subplots (also 10 m x 25m; hereafter referred as *virtual subplots*) randomly distributed across the disturbed forest (Figure 1d and e). These virtual subplots were used to evaluate the robustness of tree-mortality estimates by the three satellites in adjacent areas containing a greater variation windthrow severity (Figure 1e). The NPV values for virtual subplots were obtained using the same method as described for field subplots.

2.3. Remote Sensing Estimates of Windthrow Tree-Mortality

 doi:10.20944/preprints202305.1631.v1

We fitted a Generalized Linear Model (GLM) [66] relating *NPV* to the percentage of windthrow tree-mortality recorded in the forest inventory. The GLMs were fitted for each satellite using the binomial family for describing the distribution of residuals. We used the *logit* link function, in which linear predictors must be reversed to the scale of the observations by means of an inverse function [66].

We used the field subplots only for model fitting, thus avoiding overfitting problems for the cases in which the validation was carried using the same subplots [67]. Virtual subplots were not used for validation/training. We rather focused on evaluating the performance of the models by partitioning the *Residual Deviance* using Analysis of Variance (ANOVA). This allowed us to check which model best captured field measurements of windthrow tree-mortality (i.e., ground truth). We also used the Akaike Information Criteria (AIC, [68]), Standard Error of the Estimates (S_{yx}), Root Mean Square Error (RMSE), Residual Standard Deviation (Sigma), and the Adjusted Coefficient of Determination (R^2) computed with the Kullback-Leibler divergence formula (R^2_{KL}, [69]) as parameters for model selection. The R^2_{KL} is suitable for exponential family models (e.g. logit), which retains the informative properties of the fit due to the inclusion of regressors [69,70]. The best model was the one with the lower Residual Deviance, AIC, S_{yx}, RMSE, Sigma, and higher R^2_{KL}.

We evaluated the quality of remote sensing estimates of windthrow tree-mortality as metrics of precision/accuracy (i.e., minimum [Min], maximum [Max], median and mean) and dispersion/uncertainty (i.e., standard deviation [SD], standard error [SE] and 95% confidence interval of the mean [hereafter referred as 95% CI]). For comparing our results with those reported for other Amazon regions [2,4], we analyzed tree-mortality within categories describing windthrow severities: old-growth/undisturbed forest [≤4% of windthrow tree-mortality]; low windthrow severity [4% < windthrow tree-mortality ≤ 20%]; moderate windthrow severity [20% < windthrow tree-mortality ≤ 40%]; high windthrow severity [40% < windthrow tree-mortality ≤ 60%]; and extreme windthrow severity [> 60% of windthrow tree-mortality]).

2.4. Statistical Analysis

We checked the normality and homogeneity of field measurements (i.e., ground truth) and remote sensing estimates of windthrow tree-mortality across subplots using Shapiro-Wilk and Levene variances test, respectively. As our data were not normally distributed and field subplots were nested in the transects, we further conducted a non-parametric approach. We used the median as a comparison metric [71], and applied the Kruskal-Wallis test to assess differences on the distributions of windthrow tree-mortality values in the subplots measured in the field and remotely estimated. Differences between field and remote sensing estimates were assessed using the Mann-Whitney post-hoc test, which allows for comparing two non-paired data sets. Although the arithmetic mean is not a precise measure of central tendency from non-parametric data sets [71], we additionally reported the weighted mean values for field measurements and remote sensing estimates as supported by the Central Limit Theorem [72]. We further analyzed differences among satellites using an ANOVA followed by Tukey post-hoc test. Statistical analyses were conducted in the R 4.2.2 plataform [73] and based on a probability level of 95%.

3. Results

3.1. How Does Spatial Resolution Affect Satellite Estimates of Windthrow Tree-Mortality?

Across all field subplots (0.75 ha), we sampled 341 live and 121 dead trees. These numbers are equivalent to 616 ± 13.3 trees.ha^{-1} (all living and dead trees), 455 ± 70.2 live trees.ha^{-1}, and 161 ± 63.7 dead trees.ha^{-1} (mean ± 95% CI). The live trees were distributed in 142 species or morphotypes, 86 genera and 36 families. The mean windthrow tree-mortality measured in the field was 26.9 ± 11.1%, with a median of 13%, and minimum and maximum values of 0% and 93%, respectively (Table S3).

As reported in previous studies using ΔNPV [1,6,9], variations of windthrow tree-mortality were efficiently captured by linear models fit with *NPV* data derived from the three satellites evaluated in our study. Overall, the best agreement between field measurements and satellite estimates (i.e., lower

 doi:10.20944/preprints202305.1631.v1

Residual Deviance, AIC, S_{yx}, RMSE, Sigma, and higher R^2_{KL}) was achieved with Landsat 8, followed by Sentinel 2 and WorldView 2. This result indicates that across the entire gradient of disturbance, increasing the spatial resolution (i.e., from Landsat 8 to Sentinel 2 and WorldView 2) implied a systematic loss of quality of fit of the models. Moreover, increasing the spatial resolution did not consistently modify the intercept and slope coefficients of models. Surprisingly, all satellites showed minimum values of tree-mortality ranging from ~ 9-11% (intercept) and slope close to one (Table 1).

Table 1. Fitting summary of GLM models used to relate field with remote sensing estimates of windthrow tree-mortality in a Central Amazon forest, Brazil. AIC = Akaike Information Criteria; S_{yx} = standard error of the estimates; RMSE = root mean square error; Sigma = residual standard deviation; R^2_{KL} = Kullback-Leibler coefficient of determination.

Model	Residual Deviance	AIC	Syx	RMSE	Sigma	R²KL	Coefficients	
							a (intercept)	b (slope)
Landsat 8	125.33	183.37	0.2096	0.194	2.116	0.4342	9.08	0.9837
Sentinel 2	136.51	194.55	0.2211	0.209	2.208	0.3837	11.21	0.9719
WorldView 2	150.01	208.05	0.2234	0.219	2.315	0.3237	10.61	0.9977

Our models indicated a strong and positive correlation between NPV_{norm} and field measurements of windthrow tree-mortality ($p< 0.001$, all, Figure 3). The mean and median of satellite estimates were statistically similar for both field ($F= 0.003$ and $p= 0.99$ [mean test]; $X^2_{Kruskal\text{-}Wallis}= 3.23$ and p-value= 0.36 [median test]) and virtual subplots ($F= 0.70$ and $p= 0.49$ [mean test]; $X^2_{Kruskal\text{-}Wallis}= 1.58$ and p-value= 0.45 [median test]). Two more interesting patterns became evident by increasing the spatial resolution used for estimating windthrow tree-mortality. First, there was a general decrease in the uncertainty associated with the mean and median (decrease of standard deviation, standard error, confidence interval, and interquartile interval), which reflected the systematic increase of the number of pixels within subplots. Second, there was an increase in aggregation of estimated values in a narrower range of distribution across the disturbed landscape, which also resulted in systematic reductions on interquartile ranges (Table 2).

Table 2. Descriptive statistics for windthrow tree-mortality (%) measured from field and estimated by remote sensing data for a Central Amazon forest, Brazil. Min and Max- minimum and maximum values; Q1 and Q3- first and third median quartiles; Iqr- Interquartile range; SD- Standard Deviation; SE- Standard Error; CI- 95% Confidence Interval. *The mean of windthrow tree mortality values in the field subplots was statiscally similar among satellites due the linear modeling properties. All estimates of windthrow tree-mortality were normalized to the area of the field subplots (i.e., 10 m x 25 m) to allow comparisons among satellites.

Subplot type	Measure	Min	Max	Median	Q1	Q3	Iqr	Mean	SD	SE	CI
Field	Field	0.0	93.0	13.0	0.0	47.0	47.0	26.9	29.7	5.4	11.1
	Landsat 8	10.3	80.1	16.1	12.8	29.8	17.0	26.5*	22.5	4.1	8.4
	Sentinel 2	11.4	75.0	16.3	14.0	22.8	8.8	26.5*	21.2	3.9	7.9
	WorldView 2	12.6	80.8	18.0	15.4	22.3	6.9	26.5*	19.7	3.6	7.4
Virtual	Landsat 8	11.1	81.1	17.6	15.0	43.7	28.7	30.2	22.1	2.2	4.4
	Sentinel 2	11.7	80.2	19.5	16.2	40.9	24.7	30.3	19.5	1.9	3.9
	WorldView 2	13.1	92.0	21.2	16.8	32.2	15.4	27.4	16.1	1.6	3.2

 doi:10.20944/preprints202305.1631.v1

The sensitivity of the different satellites also varied across the windthrow tree-mortality gradient. Landsat 8 and Sentinel 2 showed a similar trend that differed from that of WorldView 2 (Figure 3a). Overall, by increasing spatial resolution, we observed a decrease in the quality of tree-mortality estimates with respect to field measurements (i.e., expressed as the R^2 relating fits and the 1:1 line, Figure 3b). Windthrow tree-mortality obtained from Landsat 8 and Sentinel 2 had a more uniform residual distribution than that of WorldView 2, which indicates that the sensitivity of the former satellites was less susceptible to bias at the extremes of the severity gradient (Figure 3c). While increasing spatial resolution led to a higher sensitivity to capture diffuse tree-mortality and potentially crown damage, it reduced the sensitivity of detecting severe windthrow tree-mortality (Figure 4).

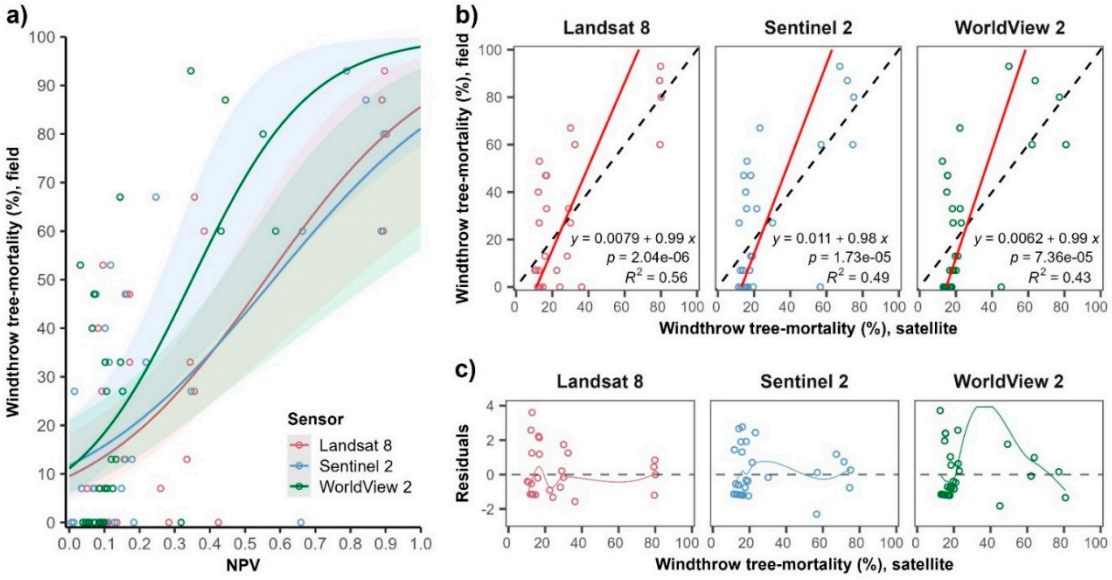

Figure 3. GLM models describing the relationship between windthrow tree-mortality measured in the field and estimated using remote sensing data. (a) Functions describing the relationship between *NPV* and windthrow tree-mortality (%) measured in the field; (b) Trend curves for windthrow tree-mortality estimated from remote sensing and measured in the field. The black dotted and red lines are the 1:1 line (perfect linear relationship) and the actual relationship between observed and estimated values, respectively; (c) Residual distribution of fitted models.

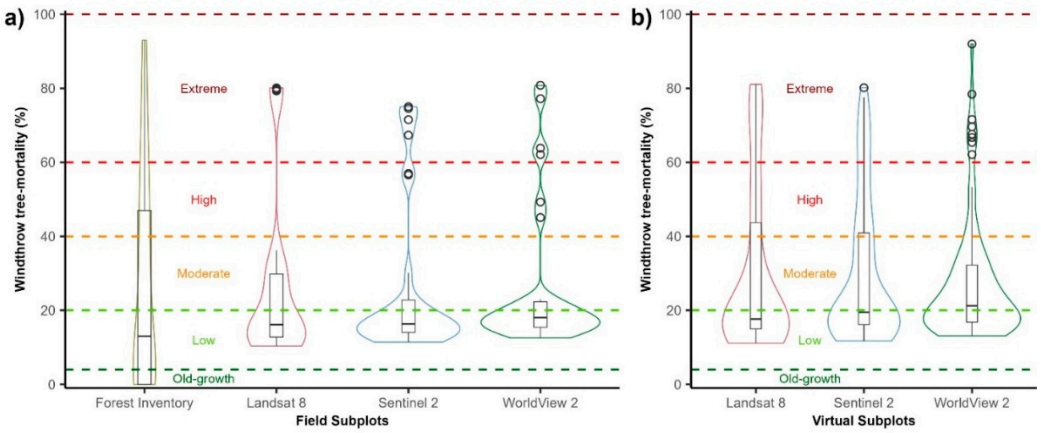

Figure 4. Distribution of windthrow tree-mortality (%) estimated from satellite data with varying spatial resolution (i.e., from 2 m to 30 m pixel). a) Windthrow tree-mortality in the field subplots. b) Windthrow tree-mortality in the virtual subplots. The hollow black circles show the outliers.

3.2. Which Sensor Produces the Most Reliable Estimates of Windthrow Tree-Mortality Across an Extent Gradient of Windthrow Severity?

Preprints.org (www.preprints.org) | NOT PEER-REVIEWED | Posted: 23 May 2023 doi:10.20944/preprints202305.1631.v1

All satellites produced consistent estimates of windthrow tree-mortality from moderate to high disturbance severity (i.e., 25% to 42% of windthrow tree-mortality). From undisturbed conditions (i.e., old-growth forest) to moderate windthrow severity the three satellites overestimated field measurements by 5-10%. From moderate to extreme windthrow severity we found the opposite pattern – underestimation between 10-15% (Figure 5a). For the virtual subplots covering a wider disturbance gradient, the remote sensing estimates were only statistically similar from low to moderate windthrow tree-mortality. From moderate to extreme windthrow tree-mortality, Landsat 8 and Sentinel 2 yielded comparable values, but these were different from those from WorldView 2 (Figure 5b). Although with greater associated uncertainties at specific ranges of tree-mortality (low to moderate and high to extreme severity), Landsat 8 and Sentinel 2 better captured the overall variation of windthrow tree-mortality over a wider disturbance gradient.

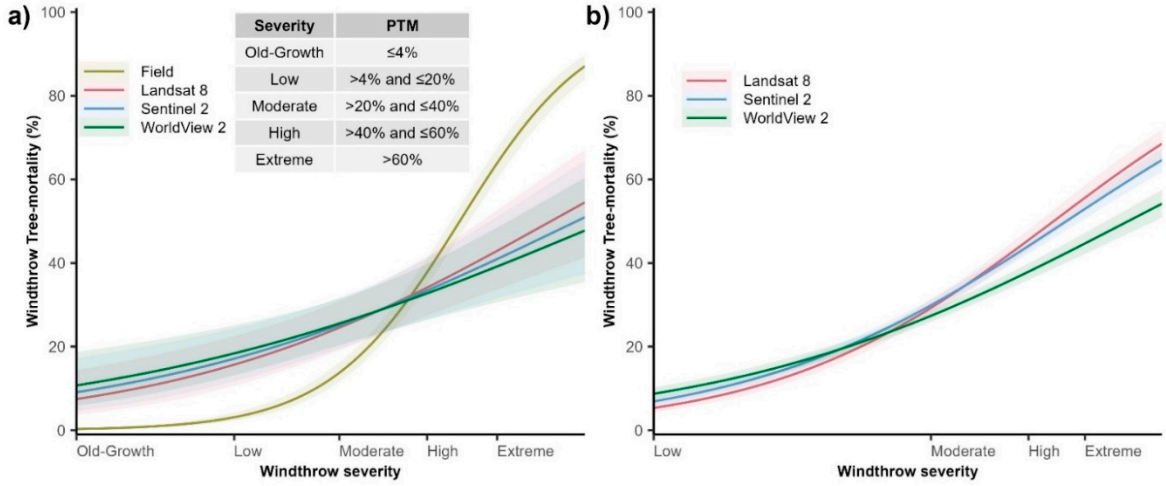

Figure 5. Percentual windthrow tree-mortality measured in the field and estimated by remote sensing data for a Central Amazon forest, Brazil. (a) Windthrow tree-mortality in Field subplots; (b) Windthrow tree-mortality in Virtual Subplots. In (a) and (b), we modeled windthrow tree-mortality estimates tendency using GLMs. The grey polygons in (a) and (b) indicate the 95% confidence interval. In the (a) plot legend, Field = Windthrow tree-mortality measured by Forest Inventory; PTM = Percentage of windthrow tree-mortality.

4. Discussion

4.1. Relating Satellite Data and Field Data

Our results showed that the sensitivity of satellites to detect low and severe windthrow tree-mortality is affected by the spatial resolution (Table 2). In windthrown areas there is an abrupt reduction in GV followed by consequent increases of NPV. Nonetheless, the NPV signal can be lost in less than a year due to the fast growing of pioneer species and survivor saplings and seedlings originally suppressed at the understory of the forest [1,7,16]. As supported by our data, the loss of the NPV signal might be critical for medium to high spatial-resolution imagery with relatively small pixel size, which are more likely to be influenced by the fast emergence of photosynthetic/green vegetation (GV) [20].

The convective storm that impacted our study region occurred about eight months (November/2015) prior to the acquisition of the satellite imagery (July/2016). Therefore, our NPV endmembers may already contain the GV sign of the regenerating forest. This was evidenced by the relatively high reflectance values in the NIR wavelength (~ 0.83 μm, Figure S9). This fast admixture of green vegetation may have contributed to the high levels of spectral mixing we observed, and this effect was systematically reduced with increasing spatial resolution (i.e., from Landsat 8 to Sentinel 2 and further WorldView 2). Although understory trees were not covered in this study, our data support that the high values of NIR attributable to the dead vegetation tend to be diluted by following

 doi:10.20944/preprints202305.1631.v1

grow of the regeneration. Again, our data support that the sensitivity for capturing such shifts tend to decrease from Landsat 8 to Sentinel 2 and WorldView 2.

The detection of tree damage and mortality using satellite data can be affected by several factors, such as canopy heterogeneity, understory density, angle-of-view/illumination and shadow effects [52,56,74]. Overall, gains in spatial resolution improve the accuracy of detecting treefall gaps [26,27,30,75,76] because in small targets the spectral information is highly influenced by geometric characteristics [25]. However, the number of pixels needed to capture the physical properties of the different surfaces comprising gaps associated with large-scale windthrows is highly determined by the spectral resolution of imagery [77]. Since the mean reflectance of a given area is strongly influenced by the material with the highest reflectance values [52], the lower the spatial resolution of the sensor (i.e., the larger pixel size), the greater the mixture of signals produced by surfaces with relatively high reflectance. However, smaller pixels can reduce these effects [56], which is supported by the higher sensitivity of WorldView 2 to capture tree-mortality in less-disturbed areas. WorldView 2 also produced higher mortality estimates than Landsat 8 and Sentinel 2 at low and moderate windthrow severity (4% < windthrow tree-mortality ≤ 40%). Given the pixel size and the comparatively larger crown diameter and area of canopy trees in our study region (mean of ~35 m^2, [78,79]), this result suggests that WorldView 2 (4 m^2 pixel area) captures vegetation damage smaller than those measured in the field.

High-resolution remote sensing models (HR-models) assume that elements in the scene are larger than scene pixels, and low-resolution models (LR-models) assume the opposite [80]. This means that the spatial arrangement of varying elements within a scene can be detected directly in HR-models because individual elements can be identified. This is usually not achieved with LR-models [14,80].

In windthrows, the process of detecting and estimating tree mortality will transit between HR- and LR-models, depending on the level of disturbance severity and the size of pixels. For example, in a moderate impacted area (e.g., assuming 50% dead trees and 50% live trees) inside one Landsat 30 m x 30 m pixel, the spatial autocorrelation among the trees is not detected because tree crowns and trunks are, in general, smaller than the pixel size. In this case, unique information (i.e., extracted from a single pixel) will represent the entire set of live and dead trees and will probably be more influenced by the highest reflectance objects [53,77]. However, in HR-models, the same area is represented by several pixels (e.g., 2 m x 2 m pixel of WorldView 2). In this case, the spatial arrangement of vegetation becomes relevant because trees are larger than the pixels, which tend to resemble their neighbors because they are likely to capture the signature of the same homogeneous target [20]. In HR-models, the varying information captured by several pixels will represent the entire set of live and dead trees. [14]. Depending on the size and severity of the windthrow in relation to the pixel size, *HR-* and *LR-models* will have different relationships between the number of dead trees in the field and the spectral/spatial information extracted from pixels of the image. Our results indicate that many pixels within the subplots provide more detail on the spectral information of the disturbance. However, tree damage (e.g., defoliation broken branches and partial loss of crown) should also be quantified in the forest inventory to maximize the higher potential sensitivity of the remote sensing data with higher spatial resolution.

A precise match between field and remote sensing data also improves the quality of tree-mortality estimates. The practical effect of this aspect is that pixels outside observational subplots may have been incorrectly compared with field data due to inaccuracy of position. Our plots were georeferenced with a navigation GPS (Garmin 64 CSx), which may have reduced the accuracy of our assessment. This effect was likely more relevant for WorldView 2. Geolocation errors for Landsat 8 are at the order of 30 m at the United States and 50 m globally [81]. For Sentinel 2 and WorldView 2, global errors are at the order of 12.5 m [82,83] and 3.5 m [84], respectively. However, previous studies using the same plot size we used here showed high correspondence between ground truth and the NPV signal obtained with Landsat [1,2]. Future studies may test the effect of increased plot sizes on the matching quality of imagery and field data. Here is important to consider logistical and safety aspects.

 doi:10.20944/preprints202305.1631.v1

As previously demonstrated, the ΔNPV metric provides a robust estimate of windthrow tree-mortality [1,2,16]. Our model fitted with WorldView 2, for which we only had the image after the windthrow, was fitted with the NPV_{norm} fraction. As supported by our results (Figure S5, Figure S6, Figure S7, Table S4, Table S5, Table S6), using NPV_{norm} for quantifying windthrow tree-mortality also produced robust and unbiased estimates. This may be a limitation for assessing patterns of tree mortality in more deciduous forests, those in highly fragmented areas or subjected to multiple exogenous disturbances. High-resolution imagery should also cover the pre- and post-disturbance conditions with the shortest possible time interval between scenes.

4.2. Trade-Off between Precision and Accuracy of Satellite Estimates

By increasing spatial resolution and consequently the number of pixels representing a given target, we observed a systematic reduction of uncertainties (SD, SE, and CI) associated with our estimates of windthrow tree-mortality (Table 2). However, reductions in uncertainty were followed by systematic reductions in the quality of model fits, mostly due to large errors at the extremes of the disturbance gradient (i.e., low, and extreme windthrow severity). This pattern suggests a trade-off between precision and accuracy [85]. In this case, precision indicates the reduction of uncertainty around the mean estimate, and accuracy indicates the closeness of the estimates in relation to the ground truth across the gradient of windthrow tree-mortality. In our study, all satellites delivered tree-mortality estimates closer to the ground truth over a restricted range of disturbance (from moderate to high windthrow severity). However, previous studies in nearby areas have shown that changes on the severity of windthrows led for strong differences in biomass loss and recovery trajectories of disturbed forests; apart from affecting biomass stocks and balance, windthrow severity was also related to long-term shifts in functional composition [1,2]. Therefore, all satellites studied here provide useful estimates within a range of severity important in the dynamics of forest recovery and contributes novel information on possible windthrow severities for transitional forests with different structure and composition as those reported in previous studies conducted in Central Amazon [1,7,36]. Future studies can test and replicate the methods used here for other forest types, structure, species composition and levels of deciduousness.

Although we equalized TOA values prior to comparing images, each satellite has a different setup for imaging angles (Nadir) and spectral resolution. The Nadir angle may affect the detection of targets with irregular surfaces [52,74], such as in windthrown forests with high amount of woody debris, survivor and pioneer trees [1]. Large angles can imply obscuration of images and consequent distortion of geometric and spectral features of targets [86–89]. The Landsat 8 images used here were acquired under Nadir ~0º, while the Sentinel 2 and WorldView 2 images were delivered with off-Nadir angles (~10.4º and ~20º, respectively). These differences may have reduced the quality of the NPV signal from Sentinel 2, and especially WorldView 2 in relation to that obtained with Landsat 8. This may be critical in relatively small gaps or at the edge of highly impacted areas, where insolation is generally lower and the crown of adjacent trees promotes stronger shading effects [24,90,91]. Apart from being usually acquired from off-Nadir angles due to acquisition costs or mission priorities, commercial high-resolution imagery such as WorldView 2 can be costly and restricted to small areas [87]. These aspects constrain the application of these for mapping windthrows and monitoring forest recovery over large regions.

Landsat 8 and Sentinel 2 have broad spectral resolution and spectral bands that span from the visible to the shortwave infrared (0.43 – 2.2 μm, [92,93]. Meanwhile, WorldView 2 has a spectrum restricted to the visible and near infrared (0.4 - 1.04 μm, [84]. Different terrain materials mimicking the spectrum of others is common and the use of more channels (i.e., bands) is a general recommendation for extracting more suitable image endmembers [20]. Thus, the lower spectral resolution of WorldView 2 may reduce the efficiency of Spectral Mixture Analysis in providing a proper NPV fraction-image.

The varying characteristics of satellites we evaluated make them appropriated for specific conditions. While Landsat 8 and Sentinel 2 are freely available and cover the entire planet, WorldView 2 has high costs and cover only specific or by-demand regions. WorldView 2 has a 1.1-

 doi:10.20944/preprints202305.1631.v1

day revisiting time [84]; Sentinel 2 has a 5-days [94] and Landsat 8 a 16-days [92]. Shorter revisiting times increases the chance of acquiring scenes shortly before and after the occurrence of windthrows. This feature is essential to mitigate the effects of the natural regeneration that can affect the NPV signal typical of windthrown forests. The high cloud cover in the Amazon for a long part of the year [95] also limits the availability of images, and shorter revisit intervals can help overcome this limitation.

Landsat has a longer-term collection of images than Sentinel 2 or WorldView 2 [96], which makes it more suitable for landscape-scale studies aiming at mapping windthrows and monitoring forest recovery over time [2,4]. However, Landsat may be inaccurate for quantifying and describing disturbance created by clusters of less than 6-8 fallen trees [16].

While Sentinel 2 is restricted for the last ~8 years, it is a suitable alternative for stand and landscape assessments aiming at greater levels of detail. As Sentinel 2 produce estimates with overall low uncertainties, it may also perform better at the edges of large events. Because of its continuity over years [94] Sentinel 2 may soon allow for longer-term analyses with higher precision.

Even with lower associated uncertainties and higher sensitivity in low-severity disturbances, WorldView 2 has a collection with limited possibilities in time and space for monitoring disturbance dynamics in the Amazon basin. Recently, the Planet NICFI initiative [97,98] has provided high resolution (3 - 5m pixel) multispectral imagery with a revisit interval of less than four days for much of the Amazon basin [99]. This offers a new possibility for describing levels and mechanisms of tree mortality, as well as for monitoring successional trajectories of forest recovery.

5. Conclusions

Increasing the spatial resolution of satellite images reduced the uncertainty of estimates of windthrow tree-mortality but did not improve their accuracy. Compared to WorldView 2 and Sentinel 2, Landsat 8 provided more reliable estimates that reflected our field measurements across an extent gradient of windthrow severity. This result highlights the feasibility of Landsat 8 for mapping windthrows and monitoring forest recovery in Amazon. To fully benefit from high-resolution images, field surveys used for model calibrations shall account for individual damage. However, high spatial-resolution satellite imagery are expensive and restricted to small areas, which may limit their application for large-scale assessments. Further studies applying high spatial-resolution imagery could be used to focus on detecting small clusters of dead trees and crown damage. This will improve current knowledge on mechanisms and rates of tree mortality, as well on associated processes regulating forest dynamics and carbon balance in Amazon forests.

Supplementary Materials: The following supporting information can be downloaded at the website of this paper posted on Preprints.org., Figure S1. General aspect of the windthrow affected area in November/2015, Figure S2. Delimitation of the central tracks of the forest inventory plots, Figure S3. Delimitation of the central tracks of the forest inventory plots, Figure S4. Delimitation of the central tracks of the forest inventory plots, Figure S5. GLM models describing the relationship between windthrow tree-mortality measured in the field and estimated using remote sensing data, Figure S6. Distribution of windthrow tree-mortality (%) estimated from satellite data using ΔNPV for Landsat 8 and Sentinel 2 with varying spatial resolution, Figure S7. Percentual windthrow tree-mortality measured in the field and estimated by remote sensing data using ΔNPV for Landsat 8 and Sentinel 2 for a Central Amazon forest, Brazil, Figure S8. Analysis routine for selecting endmembers used in Spectral Mixture Analysis and modeling, Figure S9. Spectral signature for the selected endmembers for (a) Landsat 8, (b) Sentinel 2, and (c) WorldView 2, Table S1. Reference data of density of trees in Terra Firme/Campinarana transition forest in Central Amazon, Table S2. Satellite image collection and specifications, Table S3. Forest inventory and satellite estimates for the filed subplots, Table S4. Fitting summary of GLM models used to relate field with remote sensing estimates using ΔNPV for Landsat 8 and Sentinel 2 of windthrow tree-mortality in a Central Amazon forest, Brazil, Table S5. Descriptive statistics for windthrow tree-mortality (%) measured from field and estimated by remote sensing data using ΔNPV for Landsat 8 and Sentinel 2 for a Central Amazon forest, Brazil, Table S6. Forest inventory and satellite estimates using ΔNPV for Landsat 8 and Sentinel 2 for the filed subplots.

Author Contributions: LE, RINJ and DMM planned and designed the research; RIN and DMM collected field data; LE carried data analyzes with support from RIN and DMM; LE and DMM wrote the manuscript with the support from all authors.

Funding: This research is part of the INVENTA (Interação Vento-Árvore na Amazônia), and the ATTO Project funded by the German Federal Ministry of Education and Research (BMBF contracts 01LB1001A and 01LK1602A), the Brazilian Ministry of Science, Technology, and Innovation (MCTI/FINEP contract 01.11.01248.00), and the Max Planck Society (MPG). LE was supported by the Amazonas State Research Support Foundation (FAPEAM) (Resolution no. 003/2019, INPA/COCAP call no. 10/2019). The WorldView 2 image was acquired as part of the Next Generation Ecosystem Experiments-Tropics (NGEE-Tropics), funded by the U.S. Department of Energy, Office of Science, Office of Biological and Environmental Research. The field campaigns were funded by the NGEE-Tropics.

Data Availability Statement: The data presented in this study are available on request from the corresponding author.

Acknowledgments: We thank Carlos Henrique de Sousa Celes and Raquel Fernandes Araujo for their support during the first field survey. We thank Rodrigo Geroni Nascimento, Walmes Zeviani and Maíra Conde for their support with the statistical analysis, and Fabiano Emmert his support with image processing and GIS analysis. RIN and JQC were supported by the Office of Science, Office of Biological and Environmental Research of the US Department of Energy, Agreement grant DE-AC02-05CH11231, Next Generation Ecosystem Experiments-Tropics. Finally, we are grateful for support from the Forest Management Laboratory from the National Institute of Amazon Research.

Conflicts of Interest: The authors declare no conflict of interest. The funders had no role in the design of the study; in the collection, analyses, or interpretation of data; in the writing of the manuscript, or in the decision to publish the results.

References

1. Marra, D.M.; Chambers, J.Q.; Higuchi, N.; Trumbore, S.E.; Ribeiro, G.H.P.M.; Dos Santos, J.; Negrón-Juárez, R.I.; Reu, B.; Wirth, C. Large-Scale Wind Disturbances Promote Tree Diversity in a Central Amazon Forest. *PLoS ONE* **2014**, doi:10.1371/journal.pone.0103711.
2. Magnabosco Marra, D.; Trumbore, S.E.; Higuchi, N.; Ribeiro, G.H.P.M.P.M.; Negrón-Juárez, R.I.; Holzwarth, F.; Rifai, S.W.; dos Santos, J.; Lima, A.J.N.N.; Kinupp, V.F.; et al. Windthrows Control Biomass Patterns and Functional Composition of Amazon Forests. *Global Change Biology* **2018**, *24*, 5867–5881, doi:10.1111/gcb.14457.
3. Rifai, S.W.; Urquiza Muñoz, J.D.; Negrón-Juárez, R.I.; Ramírez Arévalo, F.R.; Tello-Espinoza, R.; Vanderwel, M.C.; Lichstein, J.W.; Chambers, J.Q.; Bohlman, S.A. Landscape-Scale Consequences of Differential Tree Mortality from Catastrophic Wind Disturbance in the Amazon. *Ecological Applications* **2016**, doi:10.1002/eap.1368.
4. Urquiza Muñoz, J.D.; Magnabosco Marra, D.; Negrón-Juarez, R.I.; Tello-Espinoza, R.; Alegría-Muñoz, W.; Pacheco-Gómez, T.; Rifai, S.W.; Chambers, J.Q.; Jenkins, H.S.; Brenning, A.; et al. Recovery of Forest Structure Following Large-Scale Windthrows in the Northwestern Amazon. *Forests* **2021**, *12*, 667, doi:10.3390/f12060667.
5. Belward, A.S.; Skøien, J.O. Who Launched What, When and Why; Trends in Global Land-Cover Observation Capacity from Civilian Earth Observation Satellites. *ISPRS Journal of Photogrammetry and Remote Sensing* **2015**, *103*, 115–128, doi:10.1016/j.isprsjprs.2014.03.009.
6. Negrón-Juárez, R.I.; Holm, J.A.; Marra, D.M.; Rifai, S.W.; Riley, W.J.; Chambers, J.Q.; Koven, C.D.; Knox, R.G.; McGroddy, M.E.; Di Vittorio, A. V.; et al. Vulnerability of Amazon Forests to Storm-Driven Tree Mortality. *Environmental Research Letters* **2018**, doi:10.1088/1748-9326/aabe9f.
7. Negrón-Juárez, R.I.; Chambers, J.Q.; Guimaraes, G.; Zeng, H.; Raupp, C.F.M.; Marra, D.M.; Ribeiro, G.H.P.M.; Saatchi, S.S.; Nelson, B.W.; Higuchi, N. Widespread Amazon Forest Tree Mortality from a Single Cross-Basin Squall Line Event. *Geophysical Research Letters* **2010**, doi:10.1029/2010GL043733.
8. Nelson, B.W.; Amaral, I. Destructive Wind Effects Detected in TM Images of the Amazon Basin. *Int. Arch. of Photg. and Rem. Sens.* **1994**, *30*, 339–343.
9. Negrón-Juárez, R.; Jenkins, H.; Raupp, C.; Riley, W.; Kueppers, L.; Magnabosco Marra, D.; Ribeiro, G.; Monteiro, M.; Candido, L.; Chambers, J.; et al. Windthrow Variability in Central Amazonia. *Atmosphere* **2017**, *8*, 28, doi:10.3390/atmos8020028.
10. Negron-Juarez, R.; Magnabosco-Marra, D.; Feng, Y.; Urquiza-Muñoz, J.D.; Riley, W.J.; Chambers, J.Q. Windthrow Characteristics and Their Regional Association with Rainfall, Soil, and Surface Elevation in the Amazon. *Environmental Research Letters* **2023**, *18*, 014030, doi:10.1088/1748-9326/acaf10.
11. Roy, D.P.; Wulder, M.A.; Loveland, T.R.; C.E., W.; Allen, R.G.; Anderson, M.C.; Helder, D.; Irons, J.R.; Johnson, D.M.; Kennedy, R.; et al. Landsat-8: Science and Product Vision for Terrestrial Global Change Research. *Remote Sensing of Environment* **2014**, *145*, 154–172, doi:10.1016/j.rse.2014.02.001.

12. Coppin, P.; Jonckheere, I.; Nackaerts, K.; Muys, B.; Lambin, E. Digital Change Detection Methods in Ecosystem Monitoring: A Review. *International Journal of Remote Sensing* **2004**, doi:10.1080/0143116031000101675.
13. Goward, S.; Arvidson, T.; Williams, D.; Faundeen, J.; Irons, J.; Franks, S. Historical Record of Landsat Global Coverage: Mission Operations, NSLRSDA, and International Cooperator Stations. *Photogrammetric Engineering and Remote Sensing* 2006.
14. Woodcock, C.E.; Strahler, A.H. The Factor of Scale in Remote Sensing. *Remote Sensing of Environment* **1987**, *21*, 311–332, doi:10.1016/0034-4257(87)90015-0.
15. Coops, N.C.; Wulder, M.A.; White, J.C. Identifying and Describing Forest Disturbance and Spatial Pattern: Data Selection Issues and Methodological Implications. In *Understanding Forest Disturbance and Spatial Pattern*; Wulder, M.A., Franklin, S.E., Eds.; CRC Press: Florida, 2006; pp. 31–61.
16. Negrón-Juárez, R.I.; Chambers, J.Q.; Marra, D.M.; Ribeiro, G.H.P.M.; Rifai, S.W.; Higuchi, N.; Roberts, D. Detection of Subpixel Treefall Gaps with Landsat Imagery in Central Amazon Forests. *Remote Sensing of Environment* **2011**, doi:10.1016/j.rse.2011.07.015.
17. Negrón-Juárez, R.I.; Holm, J.A.; Faybishenko, B.; Magnabosco-Marra, D.; Fisher, R.A.; Shuman, J.K.; de Araujo, A.C.; Riley, W.J.; Chambers, J.Q. Landsat Near-Infrared (NIR) Band and ELM-FATES Sensitivity to Forest Disturbances and Regrowth in the Central Amazon. *Biogeosciences* **2020**, *17*, 6185–6205, doi:10.5194/bg-17-6185-2020.
18. Asner, G.P.; Kellner, J.R.; Kennedy-Bowdoin, T.; Knapp, D.E.; Anderson, C.; Martin, R.E. Forest Canopy Gap Distributions in the Southern Peruvian Amazon. *PLoS ONE* **2013**, doi:10.1371/journal.pone.0060875.
19. Asner, G.P.; Keller, M.; Pereira, Jr, R.; Zweede, J.C.; Silva, J.N.M. CANOPY DAMAGE AND RECOVERY AFTER SELECTIVE LOGGING IN AMAZONIA: FIELD AND SATELLITE STUDIES. *Ecological Applications* **2004**, *14*, 280–298, doi:10.1890/01-6019.
20. Adams, J.B.; Gillespie, A.R. *Remote Sensing of Landscapes with Spectral Images*; Adams, J.B., Gillespie, A.R., Eds.; 1st ed.; Cambridge University Press: New York, USA, 2006; ISBN 9780521662215.
21. Turner, M.G. Landscape Ecology: The Effect of Pattern on Process. *Annual Review of Ecology and Systematics* **1989**, *20*, 171–197, doi:10.1146/annurev.es.20.110189.001131.
22. Wulder, M. Optical Remote-Sensing Techniques for the Assessment of Forest Inventory and Biophysical Parameters. *Progress in Physical Geography: Earth and Environment* **1998**, *22*, 449–476, doi:10.1177/030913339802200402.
23. Townshend, J.R.G.; Justice, C.O. Selecting the Spatial Resolution of Satellite Sensors Required for Global Monitoring of Land Transformations. *International Journal of Remote Sensing* **1988**, *9*, 187–236, doi:10.1080/01431168808954847.
24. Asner, G.P.; Warner, A.S. Canopy Shadow in IKONOS Satellite Observations of Tropical Forests and Savannas. *Remote Sensing of Environment* **2003**, doi:10.1016/j.rse.2003.08.006.
25. Clark, D.B.; Castro, C.S.; Alvarado, L.D.A.; Read, J.M. Quantifying Mortality of Tropical Rain Forest Trees Using High-Spatial-Resolution Satellite Data. *Ecology Letters* **2004**, *7*, 52–59, doi:10.1046/j.1461-0248.2003.00547.x.
26. Clark, D.B.; Read, J.M.; Clark, M.L.; Cruz, A.M.; Dotti, M.F.; Clark, D.A. APPLICATION OF 1-M AND 4-M RESOLUTION SATELLITE DATA TO ECOLOGICAL STUDIES OF TROPICAL RAIN FORESTS. *Ecological Applications* **2004**, *14*, 61–74, doi:10.1890/02-5120.
27. Dalagnol, R.; Phillips, O.L.; Gloor, E.; Galvão, L.S.; Wagner, F.H.; Locks, C.J.; Aragão, L.E.O.C.O.C. Quantifying Canopy Tree Loss and Gap Recovery in Tropical Forests under Low-Intensity Logging Using VHR Satellite Imagery and Airborne LiDAR. *Remote Sensing* **2019**, doi:10.3390/rs11070817.
28. Fuller, D.O. Tropical Forest Monitoring and Remote Sensing: A New Era of Transparency in Forest Governance? *Singapore Journal of Tropical Geography* **2006**, *27*, 15–29, doi:10.1111/j.1467-9493.2006.00237.x.
29. Jackson, C.; Adam, E. Remote Sensing of Selective Logging in Tropical Forests: Current State and Future Directions. *iForest - Biogeosciences and Forestry* **2020**, *13*, 286–300, doi:10.3832/ifor3301-013.
30. Espírito-Santo, F.D.B.; Keller, M.M.; Linder, E.; Oliveira Junior, R.C.; Pereira, C.; Oliveira, C.G. Gap Formation and Carbon Cycling in the Brazilian Amazon: Measurement Using High-Resolution Optical Remote Sensing and Studies in Large Forest Plots. *Plant Ecology and Diversity* **2014**, doi:10.1080/17550874.2013.795629.
31. Espírito-Santo, F.D.B.; Gloor, M.; Keller, M.; Malhi, Y.; Saatchi, S.; Nelson, B.; Junior, R.C.O.; Pereira, C.; Lloyd, J.; Frolking, S.; et al. Size and Frequency of Natural Forest Disturbances and the Amazon Forest Carbon Balance. *Nature Communications* **2014**, doi:10.1038/ncomms4434.
32. Rehbein, A.; Ambrizzi, T.; Mechoso, C.R. Mesoscale Convective Systems over the Amazon Basin. Part I: Climatological Aspects. *International Journal of Climatology* **2018**, doi:10.1002/joc.5171.
33. IPCC *Climate Change 2021: The Physical Science Basis. Contribution of Working Group I to the Sixth Assessment Report of the Intergovernmental Panel on Climate Change [Masson-Delmotte, V., P. Zhai, A. Pirani, S.L. Connors, C. Péan, S. Berger, N. Caud, Y. Chen,]*; UK and USA, 2021;

34. Feng, Y.; Negrón-Juárez, R.I.; Romps, D.M.; Chambers, J.Q. Amazon Windthrow Disturbances Are Likely to Increase with Storm Frequency under Global Warming. *Nature Communications* **2023**, *14*, 101, doi:10.1038/s41467-022-35570-1.
35. Aleixo, I.; Norris, D.; Hemerik, L.; Barbosa, A.; Prata, E.; Costa, F.; Poorter, L. Amazonian Rainforest Tree Mortality Driven by Climate and Functional Traits. *Nature Climate Change* 2019.
36. Chambers, J.Q.; Negron-Juarez, R.I.; Marra, D.M.; Di Vittorio, A.; Tews, J.; Roberts, D.; Ribeiro, G.H.P.M.; Trumbore, S.E.; Higuchi, N. The Steady-State Mosaic of Disturbance and Succession across an Old-Growth Central Amazon Forest Landscape. *Proceedings of the National Academy of Sciences* **2013**, doi:10.1073/pnas.1202894110.
37. Esquivel-Muelbert, A.; Phillips, O.L.; Brienen, R.J.W.; Fauset, S.; Sullivan, M.J.P.; Baker, T.R.; Chao, K.J.; Feldpausch, T.R.; Gloor, E.; Higuchi, N.; et al. Tree Mode of Death and Mortality Risk Factors across Amazon Forests. *Nature Communications* **2020**, *11*, 1–11, doi:10.1038/s41467-020-18996-3.
38. Gora, E.M.; Esquivel-Muelbert, A. Implications of Size-Dependent Tree Mortality for Tropical Forest Carbon Dynamics. *Nature Plants* **2021**, *7*, 384–391, doi:10.1038/s41477-021-00879-0.
39. Telles, E. de C.C.; de Camargo, P.B.; Martinelli, L.A.; Trumbore, S.E.; da Costa, E.S.; Santos, J.; Higuchi, N.; Oliveira, R.C. Influence of Soil Texture on Carbon Dynamics and Storage Potential in Tropical Forest Soils of Amazonia. *Global Biogeochemical Cycles* **2003**, *17*, n/a-n/a, doi:10.1029/2002gb001953.
40. Ferraz, J.; Ohta, S.; de Sales, P.C. Distribuição Dos Solos Ao Longo de Dois Transectos Em Floresta Primária Ao Norte de Manaus (AM). In *Pesquisas florestais para a conservação da floresta e reabilitação de áreas degradadas da Amazônia*; MCT-INPA/JICA, Ed.; INPA: Manaus, AM, 1998; pp. 109–143.
41. Andreae, M.O.; Acevedo, O.C.; Araùjo, A.; Artaxo, P.; Barbosa, C.G.G.; Barbosa, H.M.J.; Brito, J.; Carbone, S.; Chi, X.; Cintra, B.B.L.; et al. The Amazon Tall Tower Observatory (ATTO): Overview of Pilot Measurements on Ecosystem Ecology, Meteorology, Trace Gases, and Aerosols. *Atmospheric Chemistry and Physics* **2015**, doi:10.5194/acp-15-10723-2015.
42. Stropp, J.; Sleen, P. Van der; Assunção, P.A.; Silva, A.L. da; Steege, H. Ter Tree Communities of White-Sand and Terra-Firme Forests of the Upper Rio Negro. *Acta Amazonica* **2011**, *41*, 521–544, doi:10.1590/S0044-59672011000400010.
43. Targhetta, N.; Kesselmeier, J.; Wittmann, F. Effects of the Hydroedaphic Gradient on Tree Species Composition and Aboveground Wood Biomass of Oligotrophic Forest Ecosystems in the Central Amazon Basin. *Folia Geobot* **2015**, *50*, 185–205, doi:10.1007/s12224-015-9225-9.
44. Oliveira, A.N. de; Amaral, I.L. do Florística e Fitossociologia de Uma Floresta de Vertente Na Amazônia Central, Amazonas, Brasil. *Acta Amazonica* **2004**, doi:10.1590/s0044-59672004000100004.
45. Luizão, F.J.; Schubart, H.O.R. Litter Production and Decomposition in a Terra-Firme Forest of Central Amazonia. *Experientia* **1987**, doi:10.1007/BF01945549.
46. Almeida, A.F. de Análise fitossociológica estrutural e composição florística da área de proteção ambiental margem esquerda do rio Negro, Manaus-AM. Dissertação (Mestrado em Ciências Florestais e Ambientais), Universidade Federal do Amazonas: Manaus, Brazil, 2012.
47. AMARAL, I.L. do; MATOS, F.D.A.; LIMA, J. Composição Florística e Parâmetros Estruturais de Um Hectare de Floresta Densa de Terra Firme No Rio Uatumã, Amazônia, Brasil. *Acta Amazonica* **2000**, *30*, 377–377, doi:10.1590/1809-43922000303392.
48. Woortmann, C.P.I.B.; Higuchi, N.; Santos, J. dos; Silva, R.P. da; dos SANTOS, J.; da SILVA, R.P. Allometric Equations for Total, above-and below-Ground Biomass and Carbon of the Amazonian Forest Type Known as Campinarana. *Acta Amazonica* **2018**, *48*, 85–92, doi:10.1590/1809-4392201700673.
49. Gorelick, N.; Hancher, M.; Dixon, M.; Ilyushchenko, S.; Thau, D.; Moore, R. Google Earth Engine: Planetary-Scale Geospatial Analysis for Everyone. *Remote Sensing of Environment* **2017**, *202*, 18–27, doi:10.1016/j.rse.2017.06.031.
50. Adams, J.B.; Sabol, D.E.; Kapos, V.; Almeida Filho, R.; Roberts, D.A.; Smith, M.O.; Gillespie, A.R. Classification of Multispectral Images Based on Fractions of Endmembers: Application to Land-Cover Change in the Brazilian Amazon. *Remote sensing of Environment* **1995**, *52*, 137–154, doi:10.1016/0034-4257(94)00098-8.
51. Shimabukuro, Y.E.; Smith, J.A. The Least-Squares Mixing Models to Generate Fraction Images Derived from Remote Sensing Multispectral Data. *IEEE Transactions on Geoscience and Remote Sensing* **1991**, *29*, 16–20, doi:10.1109/36.103288.
52. Ponzoni, F.J.; Shimabukuro, Y.E.; Kuplich., T.M. *Sensoriamento Remoto No Estudo Da Vegetação*; Ponzoni, F.J., Shimabukuro, Y.E., Kuplich., T.M., Eds.; 2nd ed.; Oficina de Textos: São Paulo-SP, 2012; ISBN 978-85-7975-053-3.
53. Somers, B.; Asner, G.P.; Tits, L.; Coppin, P. Endmember Variability in Spectral Mixture Analysis: A Review. *Remote Sensing of Environment* **2011**, *115*, 1603–1616, doi:10.1016/j.rse.2011.03.003.
54. Exelis Visual Solutions Information ENVI 5.3 2010.

55. Green, A.A.; Berman, M.; Switzer, P.; Craig, M.D. A Transformation for Ordering Multispectral Data in Terms of Image Quality with Implications for Noise Removal. *IEEE Transactions on Geoscience and Remote Sensing* **1988**, *26*, 65–74, doi:10.1109/36.3001.
56. Shimabukuro, Y.E.; Ponzoni, F.J. *Mistura Espectral: Modelo Linear e Aplicações*; Yosio Edemir Shimabukuro, F.J.P., Ed.; 1ª.; Oficina de Textos, 2017; ISBN 978-85-7975-270-4.
57. Uptike, T.; Comp, C. Radiometric Use of WorldView-2 Imagery Available online: https://dg-cms-uploads-production.s3.amazonaws.com/uploads/document/file/104/Radiometric_Use_of_WorldView-2_Imagery.pdf (accessed on 11 May 2022).
58. L3HARRIS Linear Spectral Unmixing Available online: https://www.l3harrisgeospatial.com/docs/linearspectralunmixing.html (accessed on 19 January 2022).
59. Nelson, B.W.; Kapos, V.; Adams, J.B.; Oliveira, W.J.; Braun, O.P.G.G. Forest Disturbance by Large Blowdowns in the Brazilian Amazon. *Ecology* **1994**, *75*, 853–858, doi:10.2307/1941742.
60. Adams, J.B.; Smith, M.O.; Gillespie, A.R. Imaging Spectroscopy: Interpretation Based on Spectral Mixture Analysis. In *Remote geochemical analysis: Elemental and mineralogical composition*; Pieters, V.M., Englert, P., Eds.; Cambridge University Press: New York, 1993; pp. 145–166.
61. Souza, C.M.; Roberts, D.A.; Cochrane, M.A. Combining Spectral and Spatial Information to Map Canopy Damage from Selective Logging and Forest Fires. *Remote Sensing of Environment* **2005**, *98*, 329–343, doi:10.1016/j.rse.2005.07.013.
62. Chambers, J.Q.; Asner, G.P.; Morton, D.C.; Anderson, L.O.; Saatchi, S.S.; Espírito-Santo, F.D.B.; Palace, M.; Souza, C. Regional Ecosystem Structure and Function: Ecological Insights from Remote Sensing of Tropical Forests. *Trends in Ecology and Evolution* 2007.
63. Daldegan, G.A.; Roberts, D.A.; Ribeiro, F. de F. Spectral Mixture Analysis in Google Earth Engine to Model and Delineate Fire Scars over a Large Extent and a Long Time-Series in a Rainforest-Savanna Transition Zone. *Remote Sensing of Environment* **2019**, *232*, 111340, doi:10.1016/J.RSE.2019.111340.
64. Gao, Y.; Skutsch, M.; Paneque-Gálvez, J.; Ghilardi, A. Remote Sensing of Forest Degradation: A Review. *Environ. Res. Lett* **2020**, *15*, 103001, doi:10.1088/1748-9326/abaad7.
65. QGIS Development Team QGIS Geographic Information System. *Open Source Geospatial Foundation Project* 2016.
66. McCullagh, P.; Nelder, J.A. *Generalized Linear Models.*; McCullagh, P., Nelder, J.A., Eds.; 2nd. Ed.; Taylor & Francis Group: Florida, 1989; ISBN 0-412-31760-5.
67. Hawkins, D.M. The Problem of Overfitting. *Journal of Chemical Information and Computer Sciences* **2004**, *44*, 1–12, doi:10.1021/ci0342472.
68. Murtaugh, P.A. In Defense of P Values. *Ecology* **2014**, *95*, 611–617, doi:10.1890/13-0590.1.
69. Kullback, S. *Information Theory and Statistics*; Wiley, Ed.; Dover Publications: New York, USA, 1997; ISBN 0-486-69684-7.
70. Cameron, A.C.; Windmeijer, F.A.G. An R-Squared Measure of Goodness of Fit for Some Common Nonlinear Regression Models. *Journal of Econometrics* **1997**, *77*, 329–342, doi:10.1016/S0304-4076(96)01818-0.
71. Gotelli, N.J.; Ellinson, A.M. A Primer of Ecological Statistics. *Journal of Chemical Information and Modeling* **2013**, doi:10.1017/CBO9781107415324.004.
72. Le Cam, L. The Central Limit Theorem around 1935. *Statistical science* **1986**, *1*, 78–91.
73. R Core Team R Core Team (2022). R: A Language and Environment for Statistical Computing. R Foundation for Statistical Computing 2022.
74. Goel, N.S.; Strebel, D.E.; Thompson, R.L. Inversion of Vegetation Canopy Reflectance Models for Estimating Agronomic Variables. II. Use of Angle Transforms and Error Analysis as Illustrated by Suits' Model. *Remote sensing of environment* **1984**, *14*, 77–111, doi:10.1016/0034-4257(84)90009-9.
75. Dalagnol, R.; Wagner, F.H.; Galvão, L.S.; Streher, A.S.; Phillips, O.L.; Gloor, E.; Pugh, T.A.M.; Ometto, J.P.H.B.; Aragão, L.E.O.C. Large-Scale Variations in the Dynamics of Amazon Forest Canopy Gaps from Airborne Lidar Data and Opportunities for Tree Mortality Estimates. *Scientific Reports* **2021**, doi:10.1038/s41598-020-80809-w.
76. Asner, G.P.; Palace, M.; Keller, M.; Pereira, R.; Silva, J.N.M.; Zweede, J.C. Estimating Canopy Structure in an Amazon Forest from Laser Range Finder and IKONOS Satellite Observations. *Biotropica* **2002**, doi:10.1111/j.1744-7429.2002.tb00568.x.
77. Theiler, J.; Ziemann, A.; Matteoli, S.; Diani, M. Spectral Variability of Remotely Sensed Target Materials: Causes, Models, and Strategies for Mitigation and Robust Exploitation. *IEEE Geoscience and Remote Sensing Magazine* **2019**, *7*, 8–30, doi:10.1109/MGRS.2019.2890997.
78. Peterson, C.J.; Ribeiro, G.H.P. de M.; Negrón-Juárez, R.; Marra, D.M.; Chambers, J.Q.; Higuchi, N.; Lima, A.; Cannon, J.B. Critical Wind Speeds Suggest Wind Could Be an Important Disturbance Agent in Amazonian Forests. *Forestry: An International Journal of Forest Research* **2019**, doi:10.1093/forestry/cpz025.
79. Ribeiro, G.H.P.M.; Chambers, J.Q.; Peterson, C.J.; Trumbore, S.E.; Magnabosco Marra, D.; Wirth, C.; Cannon, J.B.; Négron-Juárez, R.I.; Lima, A.J.N.; de Paula, E.V.C.M.; et al. Mechanical Vulnerability and

Resistance to Snapping and Uprooting for Central Amazon Tree Species. *Forest Ecology and Management* **2016**, doi:10.1016/j.foreco.2016.08.039.
80. Strahler, A.H.; Woodcock, C.E.; Smith, J.A. On the Nature of Models in Remote Sensing. *Remote Sensing of Environment* **1986**, *20*, 121–139, doi:10.1016/0034-4257(86)90018-0.
81. Loveland, T.R.; Dwyer, J.L. Landsat: Building a Strong Future. *Remote Sensing of Environment* **2012**, *122*, 22–29.
82. Storey, J.; Roy, D.P.; Masek, J.; Gascon, F.; Dwyer, J.; Choate, M. A Note on the Temporary Misregistration of Landsat-8 Operational Land Imager (OLI) and Sentinel-2 Multi Spectral Instrument (MSI) Imagery. *Remote Sensing of Environment* **2016**, *186*, 121–122, doi:10.1016/J.RSE.2016.08.025.
83. Trémas, T.L.; Déchoz, C.; Lacherade, S.; Nosavan, J.; Petrucci, B. Sentinel-2: Presentation of the CAL/VAL Commissioning Phase. *https://doi.org/10.1117/12.2194847* **2015**, *9643*, 94–106, doi:10.1117/12.2194847.
84. DigitalGlobe WorldView 2 Available online: http://www.engesat.com.br/imagem-de-satelite/world-view-2/ (accessed on 28 February 2021).
85. Hand, D.J. *Statistics: A Very Short Introduction*; Oxford University Press, U., Ed.; 1º Edition.; Oxford University Press: United States, 2008; ISBN 9780199233564.
86. Galvão, L.S.; dos Santos, J.R.; Roberts, D.A.; Breunig, F.M.; Toomey, M.; de Moura, Y.M. On Intra-Annual EVI Variability in the Dry Season of Tropical Forest: A Case Study with MODIS and Hyperspectral Data. *Remote Sensing of Environment* **2011**, *115*, 2350–2359, doi:10.1016/j.rse.2011.04.035.
87. Toutin, T. Review Article: Geometric Processing of Remote Sensing Images: Models, Algorithms and Methods. *International Journal of Remote Sensing* **2004**, *25*, 1893–1924, doi:10.1080/0143116031000101611.
88. Clark, M.L.; Roberts, D.A.; Clark, D.B. Hyperspectral Discrimination of Tropical Rain Forest Tree Species at Leaf to Crown Scales. *Remote Sensing of Environment* **2005**, *96*, 375–398, doi:10.1016/j.rse.2005.03.009.
89. Muller-Karger, F.E.; Hestir, E.; Ade, C.; Turpie, K.; Roberts, D.A.; Siegel, D.; Miller, R.J.; Humm, D.; Izenberg, N.; Keller, M.; et al. Satellite Sensor Requirements for Monitoring Essential Biodiversity Variables of Coastal Ecosystems. *Ecological Applications* **2018**, *28*, 749–760, doi:10.1002/eap.1682.
90. Denslow, J. Tropical Rainforest Gaps And Tree Species Diversity. *Annual Review of Ecology and Systematics* **1987**, *18*, 431–451, doi:10.1146/annurev.ecolsys.18.1.431.
91. Vitousek, P.M.; Denslow, J.S. Nitrogen and Phosphorus Availability in Treefall Gaps of a Lowland Tropical Rainforest. *The Journal of Ecology* **1986**, doi:10.2307/2260241.
92. USGS Landsat Science Available online: https://landsat.gsfc.nasa.gov/satellites/landsat-8/ (accessed on 4 August 2022).
93. European Space Agency SENTINEL-2 User Handbook Available online: https://sentinels.copernicus.eu/documents/247904/685211/Sentinel-2_User_Handbook.pdf/8869acdf-fd84-43ec-ae8c-3e80a436a16c?t=1438278087000.
94. European Space Agency Sentinel 2 Level 2A Available online: https://sentinel.https//sentinel.esa.int/web/sentinel/user-guides/sentinel-2-msi (accessed on 28 June 2021).
95. Martins, V.S.; Novo, E.M.L.M.; Lyapustin, A.; Aragão, L.E.O.C.; Freitas, S.R.; Barbosa, C.C.F. Seasonal and Interannual Assessment of Cloud Cover and Atmospheric Constituents across the Amazon (2000–2015): Insights for Remote Sensing and Climate Analysis. *ISPRS Journal of Photogrammetry and Remote Sensing* **2018**, *145*, 309–327, doi:10.1016/J.ISPRSJPRS.2018.05.013.
96. Williams, D.L.; Goward, S.; Arvidson, T. Landsat: Yesterday, Today, and Tomorrow. *Photogrammetric Engineering and Remote Sensing* 2006, *72*, 1171–1178.
97. Planet Team Planet Team Available online: https://www.planet.com/products/ (accessed on 22 April 2022).
98. Norway's International Climate and Forest Initiative Norway's International Climate and Forest Initiative Available online: https://www.nicfi.no/ (accessed on 22 April 2023).
99. Roy, D.P.; Huang, H.; Houborg, R.; Martins, V.S. A Global Analysis of the Temporal Availability of PlanetScope High Spatial Resolution Multi-Spectral Imagery. *Remote Sensing of Environment* **2021**, *264*, doi:10.1016/J.RSE.2021.112586.